Temperature-Dependent Hydrogen-Bond Geometry in Liquid Water

Kristofer Modig,[1] Bernd G. Pfrommer,[2] and Bertil Halle[1]

[1]*Department of Biophysical Chemistry, Lund University, SE-22100 Lund, Sweden*
[2]*Department of Physics, University of California, Berkeley, California 94720*

We have determined the hydrogen-bond geometry in liquid water from 0 to 80 °C by combining measurements of the proton magnetic shielding tensor with *ab initio* density functional calculations. The resulting moments of the distributions of hydrogen-bond length and angle are direct measures of thermal disorder in the hydrogen-bond network. These moments, and the distribution functions that can be reconstructed from them, impose quantitative constraints on structural models of liquid water.

PACS numbers: 61.20.–p, 61.18.Fs, 76.60.Cq

The peculiar physical properties of water have shaped much of our physical environment and the life processes it sustains. For this reason, water has been investigated in far greater detail than any other liquid [1–3]. A long-standing challenge of fundamental importance is to unravel the molecular origins of the unusual temperature dependence in the macroscopic properties of water, such as its density and compressibility [1] and the hydration enthalpy and entropy of nonpolar molecules [4]. Whereas the structure of "simple" liquids, such as Ar or CCl_4, is governed by molecular shape, water has an open, locally tetrahedral structure, maintained by a network of highly directional hydrogen bonds [1–3]. It has long been recognized that the thermal anomalies of water are related to this hydrogen-bond network [1], but it has proven difficult to transform this insight into a quantitatively accurate molecular theory of liquid water.

Pair correlation functions (PCFs) derived from x-ray and neutron diffraction [5–10] have provided important benchmarks for testing models of water structure and for developing force-fields for molecular simulation. But such PCFs can only give an isotropically averaged picture of water structure [11]. Within the temperature range of the stable liquid (at 1 atm), the positions of the nearest-neighbor peaks in the $O \cdots O$ and $O \cdots H$ PCFs are essentially invariant and the interpretation of peak broadening is confounded by overlapping (and nonseparable) contributions from hydrogen-bonded and nonbonded water molecules. In principle, these limitations can be overcome by molecular simulation, but the semiempirical force fields used in most water simulations may not be sufficiently realistic to faithfully reproduce the subtle structural changes responsible for water's thermal anomalies [12].

Considering the widely recognized importance of hydrogen bonding for the structure and properties of water, there is surprisingly little experimental information available on the temperature-dependent hydrogen-bond geometry. Models of water structure usually invoke structural motifs with well-defined hydrogen-bond geometry [13–16], often inspired by high-pressure ice polymorphs. If the distributions of hydrogen-bond length and angle in liquid water were available, preferably over a wide temperature range, such models could be tested decisively.

Our aim here is to provide this missing information. To this end, we make use of the magnetic shielding tensor $\boldsymbol{\sigma}$, which relates the applied magnetic field to the local field experienced by the magnetic moment of a water proton. The exquisite sensitivity of the shielding tensor to the local electronic environment makes it a powerful probe of hydrogen bonding [17]. Because the shielding tensor of the water proton is very nearly axially symmetric [18–20], it is essentially determined by the isotropic average $\sigma_{iso} = (\sigma_\parallel + 2\sigma_\perp)/3$ and the anisotropy $\Delta\sigma = \sigma_\parallel - \sigma_\perp$. Hydrogen bonding affects σ_{iso} mainly by depleting the electron density around the proton, whereas $\Delta\sigma$ is mostly affected by the induced magnetic field from the acceptor-oxygen electrons [18].

The shielding anisotropy has been determined in ice Ih from the inhomogeneous, dipolar-decoupled ^{1}H NMR line shape [21,22]. In liquid water, the shielding tensor is isotropically averaged by fast molecular tumbling; therefore, only σ_{iso} can be determined from the resonance frequency [23,24]. Previous attempts [23–25] to extract structural information from σ_{iso} alone were inconclusive because a rigorous theoretical link between shielding and intermolecular geometry was not available and because two observables are needed to define the hydrogen-bond geometry uniquely. However, $\Delta\sigma$ can be determined in liquid water from its second-order contribution to the ^{1}H spin relaxation rate.

Spin relaxation by rotational modulation of the shielding anisotropy is a well-known relaxation mechanism, easily identified from its quadratic dependence on the applied magnetic field [26]. Although ^{1}H spin relaxation in liquid water has been thoroughly studied over the past 50 years, the contribution from shielding anisotropy has escaped detection because, under normal conditions, ^{1}H relaxation is heavily dominated by strong magnetic dipole fields from nearby protons [26]. However, by H/D isotope dilution, the dipolar relaxation contribution can be reduced by an order of magnitude, and by also employing strong magnetic fields, the shielding anisotropy contribution can be boosted to about 25% [20]. From

relaxation time measurements at variable magnetic field (2.35–18.8 T) on a sample of D_2O doped with H_2O (proton fraction 0.0098), we have thus recently determined $\Delta\sigma$ with 1% accuracy [20]. (The secondary H/D isotope effect on the shielding is negligible.)

To derive geometrical information from $\boldsymbol{\sigma}$ we must know the shielding surface, i.e., the dependence of σ_{iso} and $\Delta\sigma$ on the nuclear configuration in the liquid. As a result of recent methodological advances, quantitatively accurate *ab initio* calculation of shielding surfaces is now feasible even for condensed phases [27,28]. To analyze the experimental data, we use shielding tensors calculated by *ab initio* density functional theory [19] for water protons taken from nine liquid water configurations generated by an *ab initio* molecular dynamics simulation at $27\,^{\circ}\mathrm{C}$ and $1.00\ \mathrm{g\,cm^{-3}}$ [29]. The shielding tensor was computed in the local density approximation with a norm-conserving local pseudopotential and the Kohn-Sham orbitals were expanded with an energy cutoff of 70 Ry [19,27]. The simulation used the gradient-corrected Becke-Lee-Yang-Parr (BLYP) density functional and a cubic supercell with 32 water molecules, giving excellent agreement with experimental PCFs [29,30].

We obtained σ_{iso} and $\Delta\sigma$ by diagonalizing the symmetrized shielding tensors of 567 protons. A four-dimensional shielding surface was then constructed by least-squares fitting to the expression

$$\sigma = A + Br_{\mathrm{OH}} + C\alpha + DR_{\mathrm{HO}}^{-3} + E\beta, \tag{1}$$

where σ denotes either σ_{iso} or $\Delta\sigma$, and the geometrical variables are defined in Fig. 1. For each proton, only one oxygen contact was included in the parametrization [31]. The fitted parameter values were for $\sigma_{\mathrm{iso}}(\Delta\sigma)$: $A = 64.81\ (50.00)$ ppm, $B = -31.64\ (-35.68)$ ppm $\mathrm{\AA}^{-1}$, $C = -4.24 \times 10^{-2}\ (3.03 \times 10^{-2})$ ppm deg^{-1}, $D = -32.8\ (88.0)$ ppm $\mathrm{\AA}^3$, and $E = 2.5 \times 10^{-3}\ (-0.134)$ ppm deg^{-1}. This parametrization features the theoretically expected [18] inverse-cube dependence on the hydrogen-bond length R_{HO} and was the most successful one among several investigated representations. Figure 1 shows ''intersections'' of the shielding surfaces along two intermolecular coordinates. As anticipated [18], $\Delta\sigma$ is a more sensitive hydrogen-bond probe than σ_{iso}. In particular, only $\Delta\sigma$ depends significantly on the hydrogen-bond angle β.

Figure 2(a) shows the experimental $\langle\Delta\sigma\rangle$ results [20], along with the isotropic shielding $\langle\sigma_{\mathrm{iso}}\rangle$, obtained by converting the chemical shift [24] to an absolute shielding scale. Within the experimental accuracy, the shielding anisotropy decreases linearly with temperature according to $\langle\Delta\sigma\rangle/\mathrm{ppm} = 28.54 - 0.0432(T/^{\circ}\mathrm{C})$ [20]. The isotropic shielding from -15 to $100\,^{\circ}\mathrm{C}$ was fitted to a cubic polynomial: $\langle\sigma_{\mathrm{iso}}\rangle/\mathrm{ppm} = 25.406 + 1.188 \times 10^{-2}T - 2.63 \times 10^{-5}T^2 + 7.1 \times 10^{-8}T^3$ with T in $^{\circ}\mathrm{C}$. For subsequent calculations, we used $\langle\sigma_{\mathrm{iso}}\rangle$ values interpolated from this polynomial at the temperatures of the $\langle\Delta\sigma\rangle$ measurements. The variation in $\langle\Delta\sigma\rangle$ and $\langle\sigma_{\mathrm{iso}}\rangle$ is entirely due to
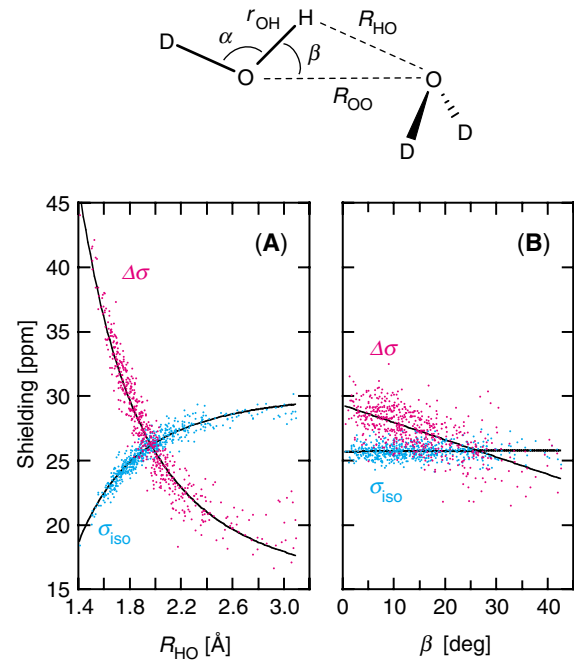

FIG. 1 (color). Dependence of the isotropic shielding σ_{iso} and shielding anisotropy $\Delta\sigma$ on the hydrogen-bond geometry in liquid water. The curves resulted from fits according to Eq. (1).

averaging over the temperature-dependent distribution of intermolecular nuclear configurations in the liquid [32]. We indicate this averaging by angular brackets.

The range of intermolecular geometries present in liquid water at any one temperature is large (see Fig. 1) compared to the variation of the mean geometry over the investigated temperature range (see below). We can therefore regard the coefficients A–E in Eq. (1) as temperature independent. In fact, a slightly more elaborate parametrization of σ_{iso} was shown to be transferable to
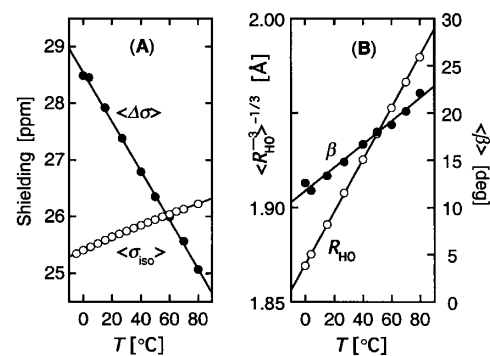

FIG. 2. (a) Temperature dependence of the configurationally averaged isotropic shielding $\langle\sigma_{\mathrm{iso}}\rangle$ and shielding anisotropy $\langle\Delta\sigma\rangle$ [20]. (b) Temperature dependence of the configurationally averaged hydrogen-bond geometry, derived from the experimental shielding data in (a) and the theoretical shielding surface in Fig. 1. The estimated experimental uncertainties, propagated from the shielding anisotropy (see Fig. 5 of Ref. [20]), are ±0.003 Å in $\langle R_{\mathrm{HO}}^{-3}\rangle^{-1/3}$ and ±2 deg in β (averaged over the nine data points).

supercritical conditions [19]. Because the mean intramolecular bond length $\langle r_{OH} \rangle$ and angle $\langle \alpha \rangle$ do not vary significantly within our temperautre range [33], we can express the configurational average of Eq. (1) as

$$\langle \sigma(T) \rangle = \sigma_0 + D\langle R_{HO}^{-3}(T) \rangle + E\langle \beta(T) \rangle,$$

where, as in Eq. (1), σ denotes either σ_{iso} or $\Delta\sigma$. The temperature-independent quantity σ_0 was determined from the experimental shielding at $27\,°C$ [see Fig. 2(a)] with the averages, $\langle R_{HO}^{-3} \rangle = 0.144 \pm 0.002\,Å^{-3}$ and $\langle \beta \rangle = 14.9 \pm 0.4$ deg, taken from the simulation at the same temperature. At the other experimental temperatures, the averages $\langle \beta \rangle$ and $\langle R_{HO}^{-3} \rangle$ can then be obtained from the measured $\langle \sigma_{iso} \rangle$ and $\langle \Delta\sigma \rangle$. The result is shown in Fig. 2(b). The linear fits are described by $\langle R_{HO}^{-3} \rangle^{-1/3}/Å = 1.870 + 0.00138(T/°C)$ $(r = 0.9999)$ and $\langle \beta \rangle/\mathrm{deg} = 11.71 + 0.1233(T/°C)$ $(r = 0.993)$. We stress that this approach does not rely on the ability of the simulation to reproduce the temperature dependence in the hydrogen-bond geometry. It requires only that the $27\,°C$ simulation adequately samples those configurations that contribute significantly to $\langle \beta \rangle$ and $\langle R_{HO}^{-3} \rangle$ in the range 0–$80\,°C$.

The observed variations [see Fig. 2(b)] in $\langle \beta \rangle$ and $\langle R_{HO}^{-3} \rangle$ reflect the temperature dependence in the underlying distribution functions $f_\beta(\beta)$ and $f_{HO}(R_{HO})$. The ab initio simulation [29] shows that $f_\beta(\beta)/\sin\beta$ is well represented (at $27\,°C$) by a Gaussian function peaked at

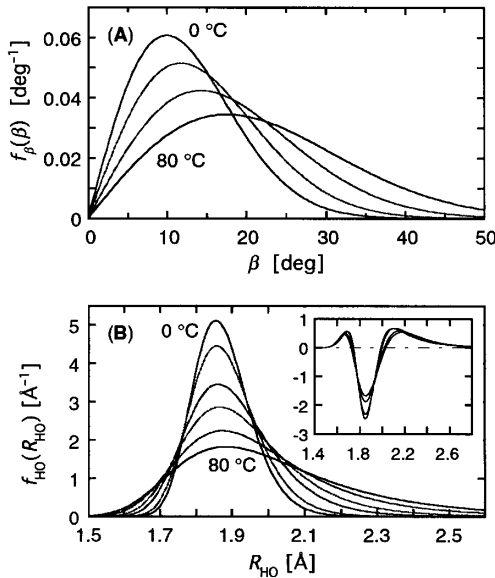

FIG. 3. Normalized distribution of (a) hydrogen-bond angle β and (b) hydrogen-bond length R_{HO}, as defined in Fig. 1. The temperatures of the curves from top to bottom are 0, 27, 50, and $80\,°C$ in (a) and 0, 4, 15, 27, 50, and $80\,°C$ in (b). The inset in (b) shows the temperature differential $\delta_{NMR} = [f_{HO}(R_{HO}, T_2) - f_{HO}(R_{HO}, T_1)]/[R_{HO}(T_2 - T_1)]$ (in units $10^{-2}\,Å^{-2}K^{-1}$) versus R_{HO} (Å). The temperature pairs, $(T_1, T_2) = (0, 70)$, $(4, 60)$, $(15, 50)$, and $(27, 40)\,°C$ from bottom to top at the minimum of the negative peak, correspond to temperature intervals of varying widths (13 to $70\,°C$) centered at $33.5 \pm 1.5\,°C$.

$\beta = 0$ and other simulation studies [11,32] show that this is the case over the full temperature range. Because the β distribution, $f_\beta(\beta) \propto \sin\beta \exp(-c\beta^2)$, involves only a single parameter c, we can convert $\langle \beta \rangle$ into the constant c or into the variance $\sigma_\beta^2 = \langle \beta^2 \rangle - \langle \beta \rangle^2$. In this way, we find for the standard deviation of the hydrogen-bond angle $\sigma_\beta/\mathrm{deg} = 6.1 + 0.064(T/°C)$ $(r = 0.993)$. The resulting distribution functions [Fig. 3(a)] resemble those obtained from computer simulations [11,34]. Note that $f_\beta(\beta)$ peaks at nonzero β because the element of solid angle increases with β even though the interaction (free) energy, at all temperatures, is minimal for a linear hydrogen bond ($\beta = 0$).

To construct the distribution function $f_{HO}(R_{HO})$ from the experimentally derived moment $\langle R_{HO}^{-3} \rangle$, we note that the ab initio simulation [27] shows that the distribution of R_{HO}^{-3} is well approximated by a Gaussian function. We take this to be the case at all temperatures. These two-parameter distributions are interrelated by

$$f_{HO}(R_{HO}) \propto R_{HO}^{-4} \exp[-(R_{HO}^{-3} - \langle R_{HO}^{-3} \rangle)^2/(2\sigma_3^2)].$$

To obtain the variance $\sigma_3^2 = \langle R_{HO}^{-6} \rangle - \langle R_{HO}^{-3} \rangle^2$, we draw on neutron diffraction [9] and simulation [34] studies, showing that the position of the first (intermolecular) peak in the PCF g_{HO} is virtually independent of temperature (in our range). Because $f_{HO}(R_{HO}) \propto R_{HO}^2 g_{HO}^{(1)}(R_{HO})$, where $g_{HO}^{(1)}$ is the contribution to g_{HO} from nearest-neighbor $H\cdots O$ pairs, we can determine σ_3 by requiring that $f_{HO}(R_{HO})/R_{HO}^2$ peaks at the same distance, $1.85\,Å$, for all investigated temperatures [8]. The resulting R_{HO} distributions are shown in Fig. 3(b). The mean and standard deviation of the hydrogen-bond length obtained from these distributions are $\langle R_{HO} \rangle/Å = 1.874 + 0.00224(T/°C)$ $(r = 0.9998)$ and $\sigma_{HO}/Å = 0.081 + 0.00330(T/°C)$ $(r = 0.9998)$.

The moments $\langle \beta \rangle$ and $\langle R_{HO}^{-3} \rangle$, and the distributions derived from them, reflect the full range of hydrogen-bond geometries present in liquid water. Even though only neighboring water molecules can be mutually hydrogen bonded, the hydrogen-bond geometry is manifested in spatial correlations of longer range. The progressive distortion of the ideal (ice-like) hydrogen-bond geometry that we observe with increasing temperature can thus be linked to the gradual disappearance of the second-neighbor peak in g_{OO} [1,5,9]. The R_{HO} distributions in Fig. 3(b) are closely related to the first intermolecular peak of the partial PCF g_{HO}. Whereas the position and integral of this peak are virtually invariant from 0 to $80\,°C$, its amplitude and shape are clearly temperature dependent [1,5–10,34–37]. The partial PCF g_{HO} can be determined by neutron diffraction with H/D substitution, but this has apparently been done at only one state point ($25\,°C$, 1 atm) in our range [8,9]. However, information about the temperature dependence of the intermolecular structure of water can also be obtained from the temperature differential of the total PCF, defined as $\delta_{PCF} = \Delta d/\Delta T$, where $d = 4\pi R\rho(T)[g(R, T) - 1]$ and $\rho(T)$ is

the molecular number density [6,7,10,35–37]. At short distances ($R < 1.9$ Å), δ_{PCF} is essentially due to the temperature dependence in $g_{HO}^{(1)}$ [6]. In the inset of Fig. 3(b), we show the quantity $\delta_{NMR} = \Delta f_{HO}/(R_{HO}\Delta T)$, which should approach δ_{PCF} at short distances [38]. Indeed, the negative peak in our δ_{NMR} is of similar amplitude and shows the same insensitivity to ΔT as the corresponding peak in δ_{PCF} [10,38].

In summary, we have characterized the hydrogen-bond geometry in liquid water from 0 to 80 °C by determining the moments $\langle \beta \rangle$ and $\langle R_{HO}^{-3} \rangle$ and reconstructing the associated distribution functions. These results reveal a substantial hydrogen-bond distortion, responsible for the gradual loss of second-neighbor spatial correlations at higher temperatures. Our results complement, and are consistent with, the isotropically averaged PCFs obtained by diffraction. We note that the magnetic shielding tensor approach introduced here can be applied to water over a wider temperature-pressure range and is, in principle, generally applicable to structural studies of hydrogen-bonded liquids and solutions.

---

[1] D. Eisenberg and W. Kauzmann, *The Structure and Properties of Water* (Clarendon Press, Oxford, 1969).
[2] F. H. Stillinger, Science **209**, 451 (1980).
[3] O. Mishima and H. E. Stanley, Nature (London) **396**, 329 (1998).
[4] N. T. Southall, K. A. Dill, and A. D. J. Haymet, J. Phys. Chem. B **106**, 521 (2002).
[5] A. H. Narten and H. A. Levy, J. Chem. Phys. **55**, 2263 (1971).
[6] I. P. Gibson and J. C. Dore, Mol. Phys. **48**, 1019 (1983).
[7] L. Bosio, S.-H. Chen, and J. Teixeira, Phys. Rev. A **27**, 1468 (1983).
[8] A. K. Soper and M. G. Phillips, Chem. Phys. **107**, 47 (1986).
[9] A. K. Soper, Chem. Phys. **258**, 121 (2000).
[10] J. C. Dore, M. A. M. Sufi, and M.-C. Bellisent-Funnel, Phys. Chem. Chem. Phys. **2**, 1599 (2000).
[11] I. M. Svishchev and P. G. Kusalik, J. Chem. Phys. **99**, 3049 (1993).
[12] M. W. Mahoney and W. L. Jorgensen, J. Chem. Phys. **115**, 10 758 (2001).
[13] S. W. Benson and E. D. Siebert, J. Am. Chem. Soc. **114**, 4269 (1992).
[14] R. C. Dougherty and L. N. Howard, J. Chem. Phys. **109**, 7379 (1998).
[15] J. Urquidi, S. Singh, C. H. Cho, and G. W. Robinson, Phys. Rev. Lett. **83**, 2348 (1999).
[16] H. Tanaka, J. Chem. Phys. **112**, 799 (2000).
[17] E. D. Becker, in *Encyclopedia of Nuclear Magnetic Resonance*, edited by D. M. Grant and R. K. Harris (Wiley, Chichester, 1996), p. 2409.
[18] R. Ditchfield, J. Chem. Phys. **65**, 3123 (1976).
[19] B. G. Pfrommer, F. Mauri, and S. G. Louie, J. Am. Chem. Soc. **122**, 123 (2000).
[20] K. Modig and B. Halle, J. Am. Chem. Soc. **124**, 12 031 (2002).
[21] A. Pines, D. J. Ruben, S. Vega, and M. Mehring, Phys. Rev. Lett. **36**, 110 (1976).
[22] L. M. Ryan, R. C. Wilson, and B. C. Gerstein, Chem. Phys. Lett. **52**, 341 (1977).
[23] W. G. Schneider, H. J. Bernstein, and J. A. Pople, J. Chem. Phys. **28**, 601 (1958).
[24] J. C. Hindman, J. Chem. Phys. **44**, 4582 (1966).
[25] I. M. Svishchev and V. V. Goncharov, Zh. Strukt. Khim. **31**, 66 (1990).
[26] A. Abragam, *The Principles of Nuclear Magnetism* (Clarendon Press, Oxford, 1961).
[27] F. Mauri, B. G. Pfrommer, and S. G. Louie, Phys. Rev. Lett. **77**, 5300 (1996).
[28] D. Sebastiani and M. Parrinello, J. Phys. Chem. A **105**, 1951 (2001).
[29] M. Sprik, J. Hutter, and M. Parrinello, J. Chem. Phys. **105**, 1142 (1996).
[30] P. L. Silvestrelli and M. Parrinello, J. Chem. Phys. **111**, 3572 (1999).
[31] Among the 567 protons, 520 are contained in the first intermolecular peak of the PCF g_{HO}, with $R_{HO} \lesssim 2.4$ Å (all these protons also have an O-H$\cdots$O angle $\theta > 120°$). The remaining 47 protons have no oxygen within 2.4 Å, but at least one oxygen in the range 2.4–3.1 Å and $\theta > 120°$. In the 15 cases where two oxygens satisfy these criteria, the one with the largest θ was chosen. Reasonable modifications of these selection criteria did not significantly alter the geometrical parameters derived from the shielding data.
[32] The configurational averages $\langle \sigma_{iso} \rangle$ and $\langle \Delta\sigma \rangle$ calculated from Eq. (1) agree to within 1 ppm with the experimental values [from Fig. 2(a)] at the simulated temperature (27 °C). We attribute this small deviation to the shortcomings of the BLYP functional and to finite-size effects [30], rather than to errors in the shielding calculation [19].
[33] K. Ichikawa, Y. Kameda, T. Yamaguchi, H. Wakita, and M. Misawa, Mol. Phys. **73**, 79 (1991).
[34] N. Yoshii, H. Yoshie, S. Miura, and S. Okazaki, J. Chem. Phys. **109**, 4873 (1998).
[35] G. Walford and J. C. Dore, Mol. Phys. **34**, 21 (1977).
[36] P. A. Egelstaff, J. A. Polo, J. H. Root, L. J. Hahn, and S. H. Chen, Phys. Rev. Lett. **47**, 1733 (1981).
[37] P. A. Egelstaff and J. H. Root, Chem. Phys. **76**, 405 (1983).
[38] At short distances, the isochoric temperature differential derived from neutron diffraction data is $\delta_{PCF} = 0.423 \times 4\pi R_{HO}\rho\Delta g_{HO}^{(1)}/\Delta T$ [6,10]. The quantity δ_{NMR} shown in the inset of Fig. 3(b) is equal to $\delta_{PCF}/0.423 + [\rho(T_2)/\rho(T_1) - 1]f_{HO}(R_{HO})/(R_{HO}\Delta T)$. Because the variation of the first term with density and the relative contribution of the second term are both less than 3%, we can compare δ_{NMR} with $\delta_{PCF}/0.423$ even though δ_{NMR} does not refer to isochoric conditions. The amplitude of the negative peak in δ_{NMR}, $(1.7-2.5) \times 10^{-2}$ Å^{-2}K^{-1}, is comparable to the corresponding amplitude, $(1.3-2.3) \times 10^{-2}$ Å^{-2}K^{-1} (after division by 0.423), in δ_{PCF} [10].